Institut für Materialprüfung,
Werkstoffkunde und
Festigkeitslehre

Masterarbeit

Roman Hofmann

Mikromechanische Ermüdungssimulation: Analyse Phaseneinfluss

Micromechanical fatigue simulation: phase influence analysis

Institut für Materialprüfung,
Werkstoffkunde und
Festigkeitslehre

Masterarbeit Nr. 760 194

Mikromechanisch Ermüdungssimulation: Analyse Phaseneinfluss

Studiengang: M.Sc. Maschinenbau

Institut für Materialprüfung,
Werkstoffkunde und Festigkeitslehre

Verfasser:	Roman Hofmann Matrikelnummer: 3144714	
Betreuer:	Dr. Ewa Soppa Dr. Christopher Kohler	IMWF / Universität Stuttgart IMWF / Universität Stuttgart
	Dr. Petra Sonnweber-Ribic M.Sc. Jannick Kuhn	Robert Bosch GmbH Robert Bosch GmbH
Prüfer:	Prof. Stefan Weihe apl. Prof. Michael Seidenfuß	IMWF / Universität Stuttgart IMWF / Universität Stuttgart
Anmeldung:	01.08.2021	
Abgabe:	31.01.2022	

Zusammenfassung

Obwohl die Forschung zur Ermüdung von Stählen bis zum Jahr 1860 [Wö60] zurückgeht, ist dies heutzutage immer noch ein bedeutendes Thema für die Industrie und die akademische Welt. Ermüdung bedeutet das ein Metall aufgrund von zyklischer Last versagt. Dabei entstehen aufgrund von Inhomogenitäten mikromechanische Verformungen in der Mikrostruktur der Metalle. Die Mikrostruktur ist die polykristalline Struktur des Metalls. Sie besteht also aus vielen einzelnen Kristallen, die Körner genannt werden und sich durch die zugrunde liegende Orientierung des Kristalls unterscheiden. Des Weiteren unterscheiden sich Körner durch ihre chemische Zusammensetzung. Den Körnern selber chemischer Zusammensetzung entsprechen eine Phase des Materiales. Zusätzliche Phasen in der Mikrostruktur erhöhen die Inhomogenität, wodurch sich die Ermüdungseigenschaften ändern. Der Einfluss Änderung soll in dieser Arbeit untersucht werden.

In dieser Arbeit werden mikromechanische Ermüdungssimulationen durchgeführt, um die Ermüdungsrissbildung in dem zweiphasigen Metall 1.4057 (X17CrNi16-2) zu untersuchen. Dazu werden mikromechanische Modelle der Mikrostruktur erstellt. Die mikromechanischen Verformungen in der Mikrostruktur werden mit dem phänomenologischen Ansatz der Kristallplastizität CP Methode bestimmt. Die resultierenden Spannungen und Dehnungen werden zur Bestimmung der Ermüdungsschädigung mit Hilfe von fatigue indicator Parameter FIP verwendet, die es ermöglichen, die Lebensdauer, d.h. die Anzahl der Zyklen bis zur Rissinitiierung, zu bestimmen.

Um den Einfluss einer zweiten Phase auf die Lebensdauer zu untersuchen, wird in dieser Arbeit, die Volumenverteilung, die Kornverteilung und die Korngröße variiert. Diese Modellvariationen werden unter dehnungs- und spannungskontrollierten Belastungen untersucht. Durch solche Veränderungen der Mikrostruktur verändern sich die Ermüdungseigenschaften und damit die resultierenden Lebensdauern.
Untersuchungen der Volumenanteils zeigten, dass eine weitere Phase die Lebensdauer beeinflusst. Die Existenz einer zweiten weichen Phase verschlechtert die Lebensdauer der Mikrostruktur. Dabei hängt der Einfluss davon ab, wie stark sich die Materialien in ihren Eigenschaften, wie Festigkeit und Härte, unterscheiden. Durch die Korngrößenstudie ergab sich jedoch, dass unter der Berücksichtigung der Hall Petch Beziehung der Einfluss der Korngröße auf die Ermüdungslebensdauer am bedeutendsten ist.

Abbreviation

bcc body-centered cubic

fcc face-centered cubic

hex hexagonal closed packed

HCF high cycle fatigue

LCF low cycle fatigue

VHCF very high cycle fatigue

UML universal material law

FIP fatigue indicator parameter

CP crystal plasticity

FEM finite element method

RVE representative volume element

SVE statistical volume elements

FFT fast Fourier Transformation

EBSD electron backscattered diffraction

Contents

1 Introduction

Failure of components can have dramatic consequences. Thus, the aim of an engineer is to design components so that failures are prevented (or at least reduced to a minimum). To do so, depending on the application, a suitable material has to be selected. Therefore, the engineer must know the deformation behavior of a material under the given loading conditions. In the transport sector, the wrong choice of material can have significant consequences. An example of this is the train accident in Eschede in 1998, which was caused by wrong designed tires (for more information on this case, please refer to the literature [Bru11]). Such an incident is due to cyclic loading, which is one of the most important loading conditions.

Materials subjected to cyclic loading fail below the static failure limit. Furthermore, not all specimens of the same material fail equally at similar load conditions, but the number of cycles to failure is scattered. This failure under cyclic load and the scatter is due to the microstructure. The microstructure of metals consists of a polycrystalline structure; it is dived in many grains that differ by their crystallographic orientation. Due to the polycrystalline structure, even single phase metals are heterogeneous. Therefore under load, local deformations in the microstructure occur, damaging the material and lowering the lifetime. This heterogeneity is further increased by a second phase. A phase is anything homogeneous and physically distinct part of the metal, which differ in their chemical composition and the arrangement of the atoms [Ao74].

The influence of microstructure on fatigue can be determined by the crystal plasticity (CP) method, which is a mesoscopic approach to simulate the micromechanical behavior. With the help of fatigue indicator parameters FIPs and corresponding critical values, damage in the microstructure for each of its phases can be determined. Multiple investigations [Boe16, BSE17] deal with the fatigue of metal and use the effectiveness of the FIP method.

Those investigations mainly refer to single-phase microstructures. However, this does not generally apply to all metals since, as already mentioned, they can consist of several phases. With each additional phase, the inhomogeneity increases, which affects the lifetime of a metal. Therefore, this work analyzes the influence of a second phase on crack initiation.

This work aims to determine how different phases in the material affect crack initiation under cyclic loading. For this purpose, many models are created, which represent a statistical part of the researched material. These models are used to determine the number of cycles until crack initiation. Changing specific parameters will determine

how the different phases affect each other. Primarily, the volume fraction occupied by the individual phases is varied, and thus, the influence of the individual phases is determined. Independently of this, the influence of the grain size is investigated under consideration of the Hall-Petch equation. By altering these microstructural properties, it is aimed to determine how two different phases affect each other and under which aspects a multiphase material is most likely to fail.

2 Fundamental concepts

2.1 Microstructure and deformation behavior of metals

Although metals are considered homogenous on a macroscopic scale, this assumption does not hold on the microscale. However, metals in their solid-state are a composition of multiple crystals, which strongly affect the properties of the metal. The multicrystalline structure is created since each of the crystals can be distinguished due to the alignment and arrangement of the atoms [Got14]. The term crystalline structure of metals refers to the fact that the atoms are arranged in a repeating configuration in three-dimensional space. The minor repetitive arrangement is called a unit cell, defined by the distance and angles between the atoms. For crystalline structures, different manifestations exist. Lattice systems describe the grouping of crystal structures. For each of the seven lattice systems there exist up to four possible ways to arrange crystal structures with in a repetitive pattern, leading to the 14 bravais lattices [Bra50].

The metallic elements crystallize for the most part in three lattice types. The body-centered cubic (bcc), the face-centered cubic (fcc), and the hexagonal closed packed (hex) which are visualized in Figure 2.1. Many properties, especially the mechanical ones, are related to the crystal structure. Due to the common appearance of those lattice types, they are the most frequently considered structures for metals [Got14].

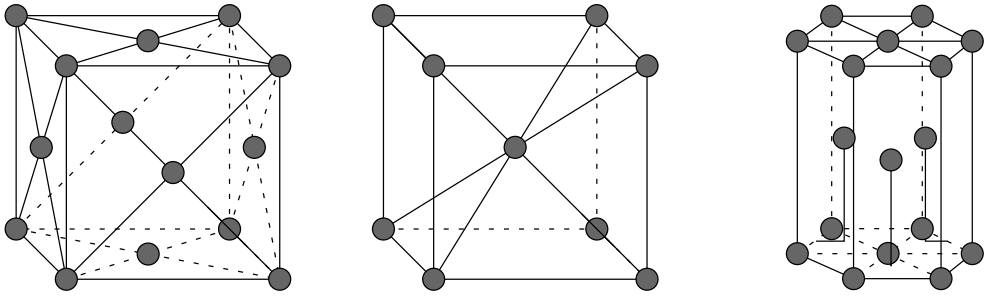

(a) fcc (b) bcc (c) hex

Figure 2.1: Schematic representation of typical unit cells manifestations [Got14]

The loading of a metallic material leads to different responses, influenced by the crystalline structures. Depending on the magnitude of the load, elastic or plastic deformation occurs. The elastic deformation describes a reversible deformation determined by the nature of the metallic bond. It can, for example, be characterized by the linear relationship of strain and stress in Hooke's law. On the macroscopic scale, at elastic deformation the component returns to its original shape after the load is removed.

When elastic deformation of a crystallographic lattice is observed, load shifts the lattice to such an extent that the lattice returns to its initial configuration at the vanishing of the load. However, if the applied load on the crystal lattice is further increased and exceeds a limit, the metallic bonds between the atoms break. The atoms move further by one atom in the lattice along a so-called slide plane. From this stage the lattice does not return to its initial configuration at the vanishing of the load. This kind of deformation is called plastic deformation, which follows the elastic response. Plasticity generally describes the irreversible part of the deformation after the load is removed.

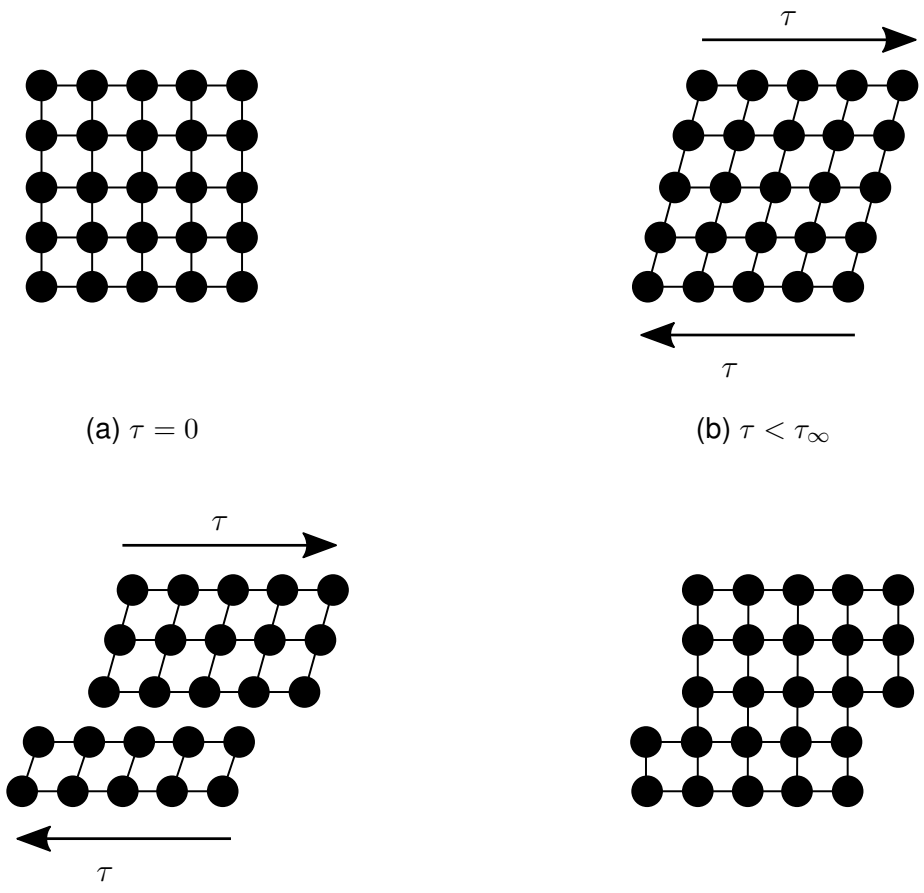

(a) $\tau = 0$ (b) $\tau < \tau_\infty$

(c) $\tau > \tau_\infty$ (d) $\tau = 0$

Figure 2.2: Plastic deformation as the result of shifting the whole upper part at once by one atom [Sch20].

The deformation of a perfect two-dimensional lattice is shown schematically in Figure 2.2. Figure 2.2b shows elastic deformation of the lattice since it returns to its original configuration with the vanishing of the load. When the load exceeds specific critical shear stress, the plastic deformation occurs, as visualized in Figure 2.2c, such afterward, the lattice re-orders in a new configuration. Theoretical estimation of the shear stress limit, made by Cottrell [Cot54], showed that in comparison to experi-

ments, the theoretical value is several orders of magnitude higher than the observed yield strength.
An explanation for this was derived by separately in 1934 by Orowan [Oro34], Polanyi [Pol34], and Taylor [Tay34]. Instead of moving *all* atoms at once in the direction of the applied shear stress, atoms move one by one. They attributed this effect to so-called dislocations. A dislocatioin is a one dimensional defects in the lattice and is interpreted as the cause of plastic deformation, representing a particular feature of metals.

Although proving this theory with electron-optical experiments was done by Hirsch [HHW56], previous studies confirmed that dislocations must exist. One of the studies was done by Bragg in 1974 [BN47]. Bragg created a model of a two-dimensional lattice. The model consists of a number of bubbles of the same size, which can move freely on the water surface. In the model, the bubbles gathered and arranged in a lattice. However, this lattice was not perfect, it has shown some imperfections that interrupted the uniform distribution. These imperfections represent the suspected dislocations. Furthermore, by distorting the bubble lattice, it was possible to see how the dislocations move, disappear and new ones emerge. Thus, brag's model was a first illustration of metals' plastic deformation due to the existence of dislocations. Further kinds of defects can exist in the lattice, which are distinguished by their dimension, which will not be discussed further. For further information about defects please refer to the literature [AHL17].

An analogy for the reduced resistance against plastic deformation is shown in Figure 2.3. Instead of simultaneous motion within the whole slip plane, the integration of dislocation as a line defect allows the consecutive motion of an inserted half-plane, as shown schematically in Figure 2.3. Thereby is visualized that the shear stress needed for the movement of atoms becomes much smaller with the existence of dislocations in the lattice. It is much easier to move a rug by running waves than dragging a rug as a whole.

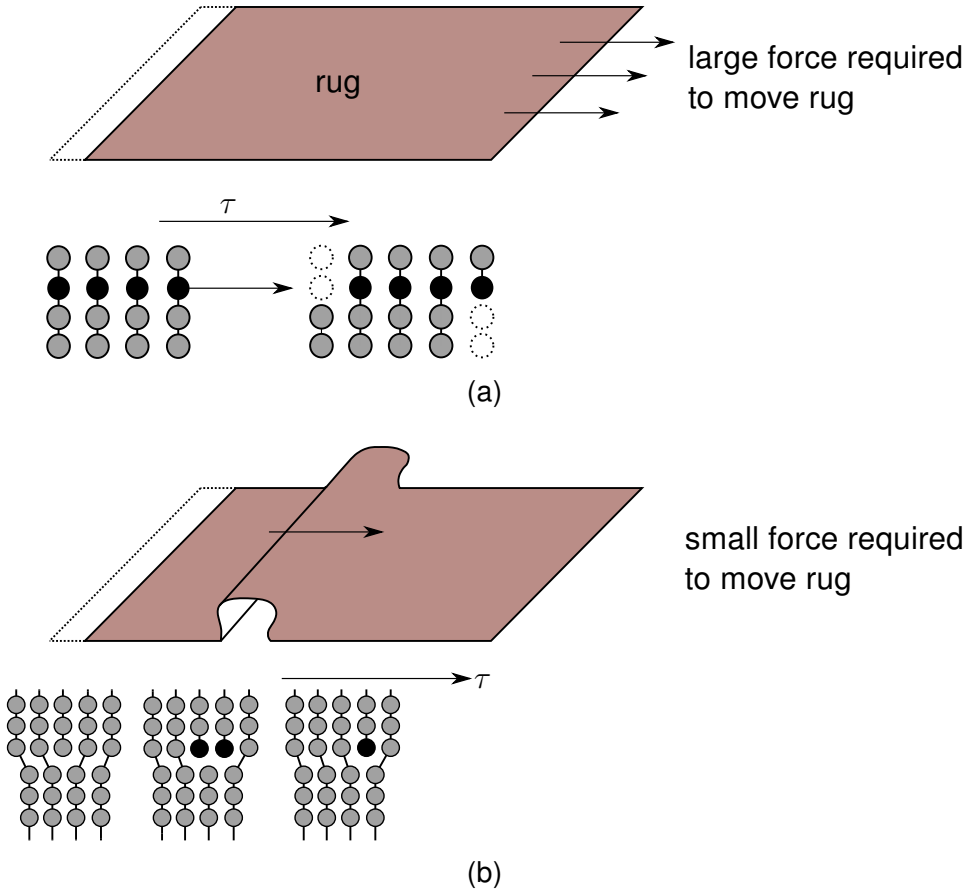

Figure 2.3: Deformationanalogy of a crystalline structure by (a) rigid slip and (b) dislocation motion [Kru07]

Dislocations do not move in arbitrary directions in the lattice. Rather they move on predifined planes in explicit directions. The accumulation of dislocation movement is called slip, the combination of plane and direction slip is called slip systems [HB11]. On those slip planes, the atoms are most densely packed, and therefore the stress required to move the dislocations is lowest. For a slip plane, there are corresponding directions where the movement of dislocation in a slip system takes place. Those slip directions describe a direction with the atoms most closely spaced. Thus the path to the next lattice site is the shortest.

For an fcc lattice, twelve slip systems exist, consisting of the four most densely packed $\{111\}$-planes and three $\langle 110 \rangle$-directions for each of the slip planes. In comparison, there are 48 slip systems in bcc-latices. The bcc has compared to the fcc no densely packed slip planes, thus the slip systems consist of only the slip direction $\langle 111 \rangle$. Therefore the 48 slip systems on which plastic slip may occur are created by the

six $\{110\}$-planes, each with two $\langle 111\rangle$-directions, twelve $\{112\}$-planes, and 24 $\{123\}$-planes. If the deformation follows only a fixed direction and no fixed slip plane, the mode is called pencil glide. Slip Systems for bcc and fcc is schematically visualized in Figure 2.4.

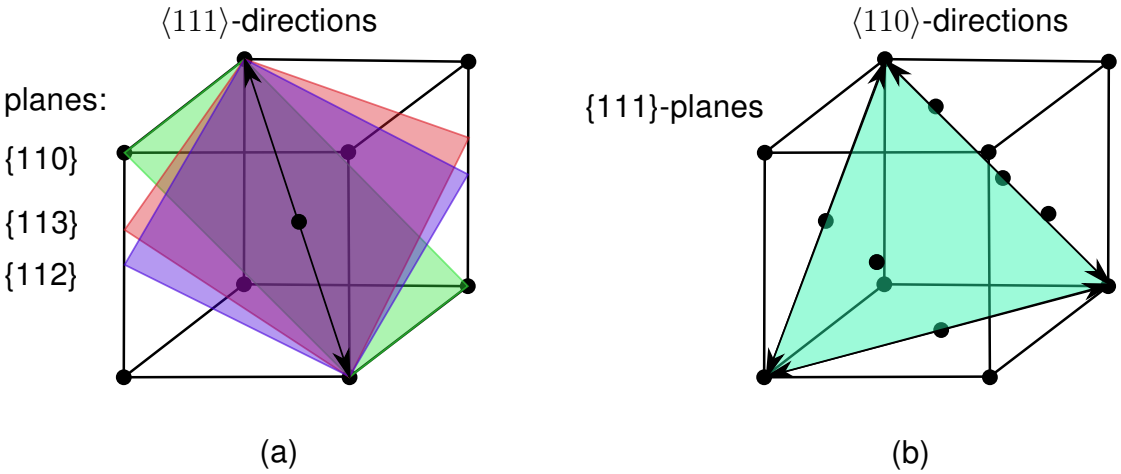

Figure 2.4: Visulatisation of different slip systems (a) bcc (b) fcc [Kru07]

The crystal's slip systems describe the planes and directions on which the atoms move when a certain shear stress is applied. The shear stress on a slip system τ^{θ} which is applied by a unaxial tension can be formulated according to Schmid's law [Got14]

$$\tau^{\theta} = \sigma_n cos(\phi^{\theta}) cos(\lambda^{\theta}) \tag{2.1}$$

where σ_n is unaxial tension on a slip system $theta$. λ^{θ} and λ^{θ} characterize the angle between the direction of σ_n, the slip plane normal and slip direction. The polycrystalline property of metals denotes that metals consist of multiple crystal structures that differ in orientation. Thus,in the entirety of the metals, multiple more slip systems exist in which deformation occurs in regard to a global coordinate system. Taking into account Schmidt's law, this means that in the individual crystals different shear stresses act on their slip systems. Therefore, the direction of the load applied to the crystal lattice is influential for the lattice's resulting elastic and plastic deformation.
These crystals, or grains, are seperated by so-called grain boundaries. The totality of the different grains which are a part of a metal is called microstructure. Nevertheless, as metallic components typically consists of a numerous grains with different orientations, the overall macroscopic behavior appears isotropic. But on the microscopic level, each grain has its orientation and responds differently when a load is applied to the microstructure. This means the material is anisotropic on the microstructural

scale. Small loads, macroscopic below the yielding stress, can damage the material by the underlying anisotropic property. The damage occurs in the microstructure since the load may exceed critical stress and strains for single grains, which depends on the grain's orientation. The microstructure's morphology leads to the problem that repetitive loads, typically smaller than the yielding stress, slowly damage the material until fracture.

2.2 Cyclic load

As mentioned in subsection 2.1, small macroscopic deformation can lead to local stress and strain peaks in the microstructure of metals due to the anisotropic microstructure of metals. Therefore, such small deformations can damage the metal without exceeding the macroscopic yielding strength. During one cycle, there might not be any damage on component scale, while within the microstructure there is already plastic deformation occuring. Damage from the microscopical plastic deformation accumulates and thus lead to failure of the component after a number of cycles. The effect of cyclic loads on the micromechanical damage is the main focus of this work.Thereby the damage on the material by cyclic loads is called fatigue [Sur98].

The most common experiments to characterize cyclic material behavior investigate the material's stress-strain response under defined cyclic loading amplitudes. The load is controlled by a stress amplitude σ_a or the strain amplitude ε_a. The hysteresis loop shows the resulting relationship between stress and strain in a single load cycle. Loading types of controlled cyclic experiments are characterized by the ratio of highest and lowest loading (σ_{max}, σ_{min}, ε_{max}, and ε_{min}). The stress ratio (R_σ) for the stress-controlled and strain ratio (R_ε) for the strain-controlled investigation is defined as:

$$R_\sigma = \frac{\sigma_{max}}{\sigma_{min}} \tag{2.2}$$

$$R_\varepsilon = \frac{\varepsilon_{max}}{\varepsilon_{min}} \tag{2.3}$$

Typical loading ratios are, for example, pure alternating loading at a ratio $R = -1$ with equal tensile and compressive loads, which implies there is no mean strain and consequently no mean stress. When only tensile load is applied, the load ratio results in $R = 0$, which is called pure threshold load. On the contrary, it is called pure compressive load.
Figure 2.5 schmeatically shows a stress-strain hysteresis under strain-controlled load-

ing with $R = -1$, which represents the corresponding material response. Primary hysteresis information can be obtained from the hysteresis curve [Chr13]. For one, the maximum load reversal point after tension relief (ε_{max},σ_{max}) and minimum load reversal point after pressure relief (ε_{min},σ_{min}). The difference between these values results in the strain and stress oscillating width ($\delta\varepsilon$, $\delta\sigma$). The strain oscillating width can be divided into elastic and plastic strain components ($\delta\varepsilon^{el}$, $\delta\varepsilon^{pl}$). In the mid of the stress amplitude, the medium stress can be determined from the stress extremes, which in this example signifies a stress ratio of $R \neq -1$.

Over time, the cyclic stress-strain hysteresis might change. Such differences of the hysteresis occur, even though the load and material properties has not changed. Under cyclic loads repetitive flow leads to dislocation interactions. Dislocation interactions might lead to softening or hardening of the metal. Those transient effects change the shape of the hysteresis curve, others change the position [Chr13]. Under strain-controlled test, depending on the initial situation, with increasing test duration hardening increases the stress amplitude of the hysteresis loops (Figure 2.6a). On the other side softening decreases the stress amplitude (Figure 2.6b).

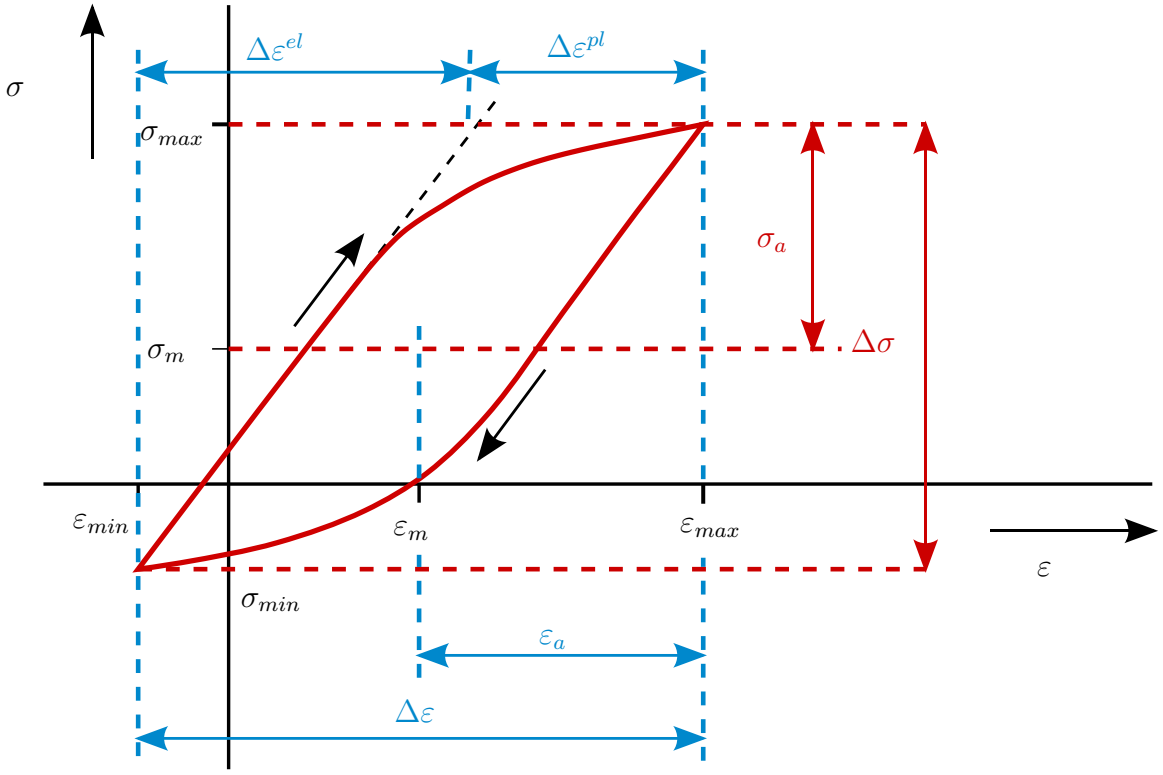

Figure 2.5: Representation of hysteresis loop with characteristic values [RHB12]

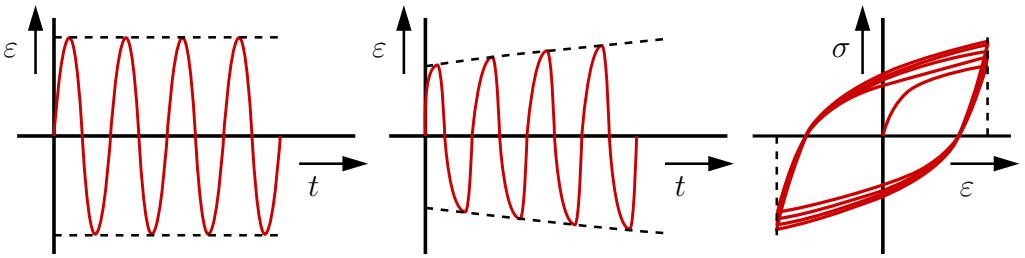

(a) Cyclic hardening

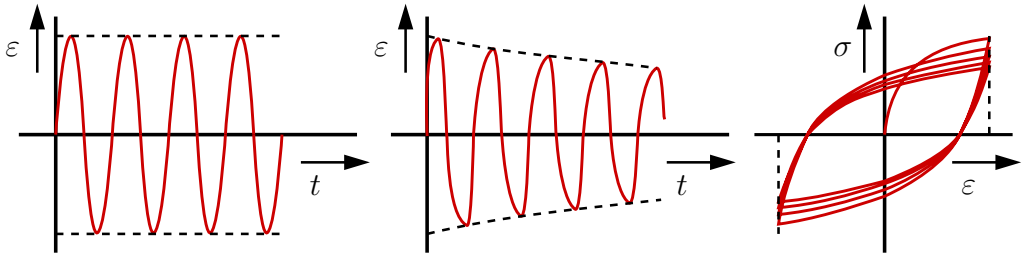

(b) Cyclic softening

Figure 2.6: Kinematic hardening [RHB19].

Cyclic loading causes a rearrangement of the preexisting dislocation structures. Under the repeated dislocation rearangement formation of new dislocations might occur . Such arrangement with increased number of dislocations are less resistant to further cyclic deformation. Those dislocation formation is the background of softening, which lowers the material's strength. Conversely the elasto-plastic cyclic deformation might cause an increase in dislocation density and a reduction of dislocation mobility. The stress response is therefore higher since the repeated dislocation annihilation and accumulation increases the strength of the metal [Sch20]. A variant to represent this behavior is described in Section **??**.

A additional phenomenon can be seen in strain-controlled tests. At an initial mean stress (σ_m) different from zero, the resulting mean stress, throughout loading cycles, may decrease down to zero [FCFR20].

As long as the mean stress differs from zero, a load in one direction may be greater than the load in the opposing direction. At a mean stress> 0 tensile load is greater than compression load. The disbalance leads to additional plastic strain increments [RHB12]. Due to those additional processed energy the loads are shifted. When the mean stress of $\sigma_m = 0$ is finally reached, these processes are in equilibrium again. Calling this phenomenon cyclic relaxation and the counterpart in the stress-controlled case is called cyclic creep. For more information about creep in polycrystalline materials, please refer to Hutchinson [Hut76].

2.2.1 Fatigue in metals

Failure of material occurs under static and cyclic loads. Components exposed to cyclic loads tend to fail at lower loads than the material's yield stress. Consequently, typical material properties used to design components under static loads are not safe to use under cyclic loads. Fatigue denotes the temporal damage and failure of a material, which for metals is a sequence of microstructural phenomena due to anisotropy in the microstructure. The number of cycles describes the fatigue behavior of metals until failure under defined loads and environmental conditions. The number of cycles until failure is henceforth called lifetime. Whereby failure can differently be described, depending on the extent of a crack.

The fatigue properties of a metal are often determined by loading the material cyclic with a specific stress amplitude until failure. In this process, the lifetime of the metal differs despite the same loading amplitude and the same environmental conditions. This scatter is visualized schematically in a Wöhler curve in Figure 2.7 which results after a statistical evaluation of several samples. The diagram plots the stress amplitude over the fatigue time, whereas it describes at which number of cycles a metal tends to fracture. Red dots in the figure represent samples under the same stress amplitude. Furthermore, the area between the dashed curves schematically shows the scatter range resulting from many samples. The scattering of the lifetimes is due to the underlying microstructure of the metal. The microstructure between two samples is not the same; their grains are differently positioned and oriented. Those microstructural differences can result in different local stresses in the same area of two samples, leading to different lifetimes.

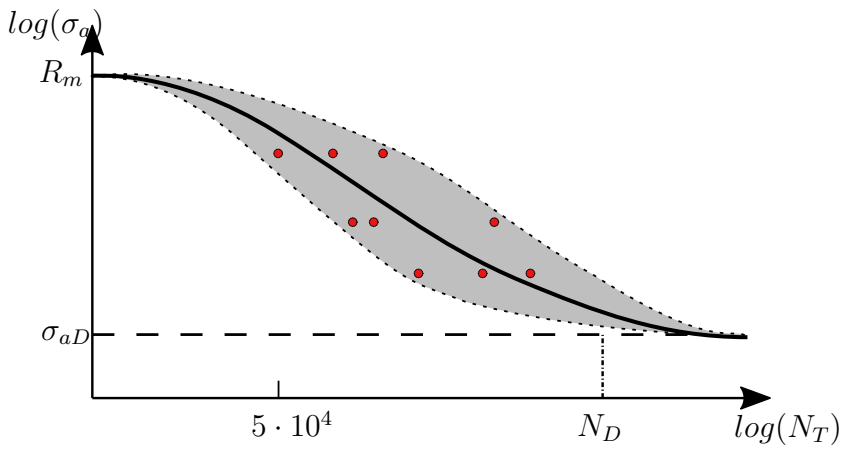

Figure 2.7: Schematic visualization of determination fatigue stress curve with scattering samples marked with red circles

The background of microstructural failure is the inhomogeneity of the microstructure. In the microstructure, the inhomogeneity is caused by the anisotropic grains, which are oriented differently. The inhomogeneity is increased again in a multiphase material. Due to the different material properties of the phases, two grains with the same orientation would behave differently under identical loading. These microstructural inhomogeneities lead to local stress accumulation, where the yield strength is exceeded and thus damages the material by plastic deformation [Sur98]. Those deformations under cyclic loads are caused by the accumulation of small dislocation movements, which lead to persistent slip bands when the dislocation movements can not move back to their initial position [San13]. Persistent slip bands are possible nucleation points for cracks. Such slip bands create boundaries to the low deformed matrix at which dislocations are gathering due to an inhomogeneous strain distribution [Ell97]. The elastic and plastic heterogeneity of grains increases the possibility of finding the crack initiation point at the grain boundaries since, at these points, local stress and strain peaks are situated.

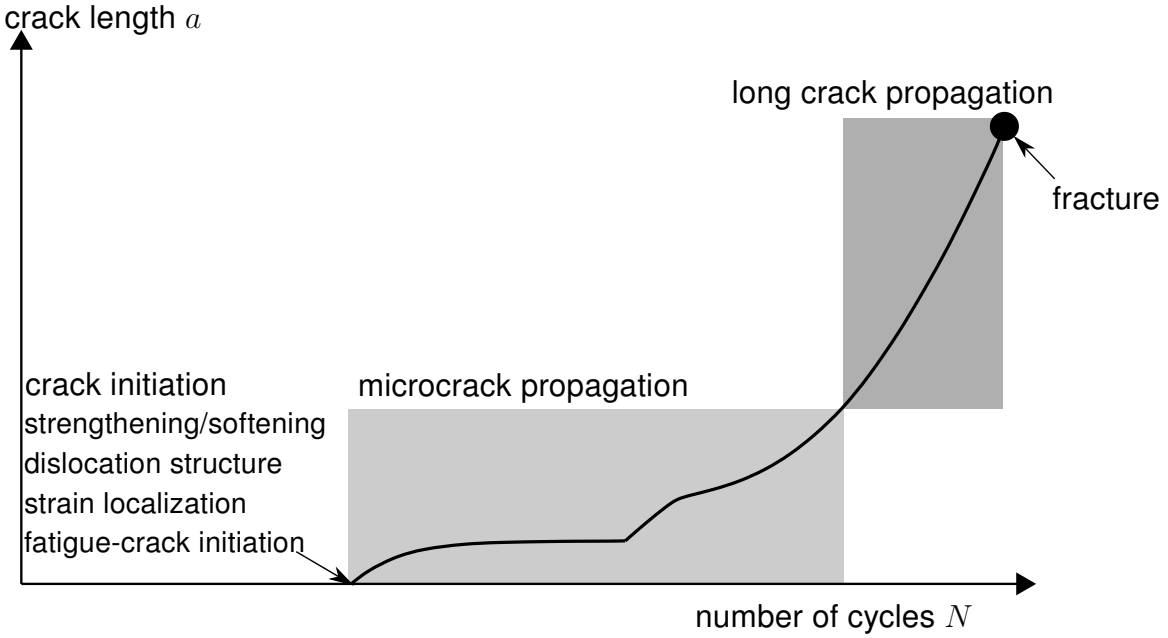

Figure 2.8: Development of fatigue damage in polycrystalline metals and alloys [Kru07].

A crack develops over several stages and must first be initiated by the local deformations in the microstructure. The short crack growth or microcrack propagation, as seen in Figure 2.8, directly follows the crack initiation. With increasing crack length, the influence of microstructure decreases, and thus the crack propagates perpendicular to the load direction. The third phase is shown schematically in Figure 2.8 as long crack propagation. The long crack Propagation describes cracks on the macroscopic

scale, with the finally fractured material when the crack exceeds a critical length regarding the load.

The different phases are combined as McDowell and Dune [MD10] proposed to a total fatigue lifetime N_T, consisting of the number of cycles N for each step in the fatigue process. The total fatigue life results from the following equation.

$$N_{\mathrm{T}} = N_{\mathrm{inc}} + N_{\mathrm{prop}} \tag{2.4}$$

where N_{inc} is the number of cycles for fatigue crack initiation and N_{prop} the number of cycles for fatigue crack propagation. This equation is a shortened form according to the equation of McDowell and Dune, in which the individual components are further divided.

Since considering only the crack initiation is in the scope of this work, for more information on the second and third phases of fatigue damage, please refer to Krupp [Kru07].

2.2.2 Empirical fatigue life predictions

For component design with regard to fatigue, it is essential to know the fatigue properties of a material. Therefore experiments are carried out for fatigue damage description. This was first done by Woehler in 1860 [Wö60]. Based on different N_{T}, three fundamental fatigue regimes exist, which depend on the magnitude of load. Figure 2.9 shows a schematic of the Wöhler curve of a material and how the three regimes are classified.

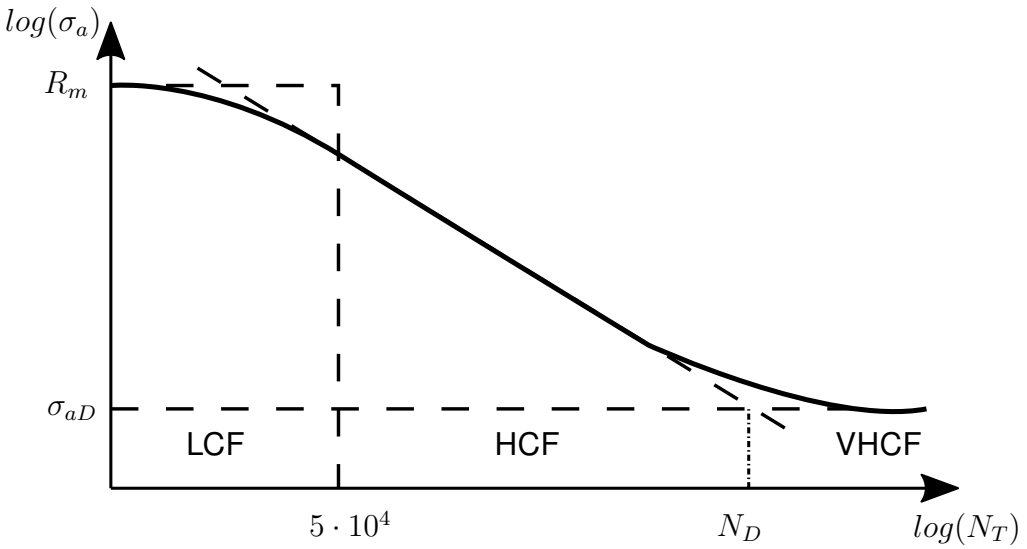

Figure 2.9: Schematic visualization of stress-lifetime diagram [Wö60]

The regime for $1 < N_\mathrm{T} < 10^4$ is called Low cycle fatigue (LCF). From a macroscopic point of view, the fatigue behavior of the component is dictated by elastoplastic material behavior. Within the High cycle fatigue (HCF) regime, with $10^4 < N_\mathrm{T} < 10^7$ number of cycles, the fatigue properties are mainly determined by the elastic behavior. In some cases, metals also fail with several cycles above the HCF regime. This regime is called Very high cycle fatigue (VHCF) with $N_\mathrm{T} > 10^9$ number of cycles and occurs below the fatigue limit. Characteristic for VHCF is the transition of nucleation sites which are more likely to be found at the surface to the bulk.

The total fatigue life N_T is often determined with phenomenological and empirical methods, considering measurable macroscopic variables, e.g. the applied stresses and strains. One approach to predict fatigue life is the cumulative fatigue damage theory, which refers to the initiation and propagation of a critical crack until failure. The fatigue life is linked to the nominal stress amplitude. Thus, fatigue specimens are stressed under constant stress amplitude until a failure criterion is attained or a predefined number of cycles is reached. If a specimen is loaded with a small amplitude primarily elastic strains evoke in the material. Thus, for some metals, an exponential relationship of the sustained stress amplitude from the number of load cycles to failure $2N_T$ is observed. The so-called fatigue strength range (Basquin [Bas10]) describes this correlation, according the HCF range, with

$$\sigma_a = \sigma_f^{'}(2N_T)^b \tag{2.5}$$

with the models parameter $\sigma_f^{'}$ and b. $\sigma_f^{'}$ is the fatigue strength coefficient, and b is the fatigue strength exponent for a metal. The Basquin law describes a lifetime curve in the HCF regime, thus not considering the earlier fatigue. Nevertheless, the LCF regime, where besides elastic strains also high plastic strains occur, has to be taken into account.

Coffin and Manson, independently of each other, described the fatigue behavior in LCF regime, which takes into account the plastic strains with the equation:

$$\varepsilon_{a,p} = \varepsilon_f^{'}(2N_T)^c \tag{2.6}$$

with the models parameter $\varepsilon_f^{'}$ and c. $\varepsilon_f^{'}$ is the fatigue ductility coefficient and c the fatigue ductility exponent.

Combining the elastic and plastic strain amplitudes to $\varepsilon_a = \varepsilon_{a,e} + \varepsilon_{a,p}$ and modifying Equation 2.5 by $\varepsilon_{a,e} = \sigma_a/E$ allows to combine the Manson-Coffin and Basquin relationships into one equation.

$$\varepsilon_a = \frac{\sigma_f^{'}}{E}(2N_T)^b + \varepsilon_f^{'}(2N_T)^c \tag{2.7}$$

Figure 2.10 visualizes this relationship in a double logarithmic plot. Where the straights represent either the elastic or plastic part of Equation 2.7.

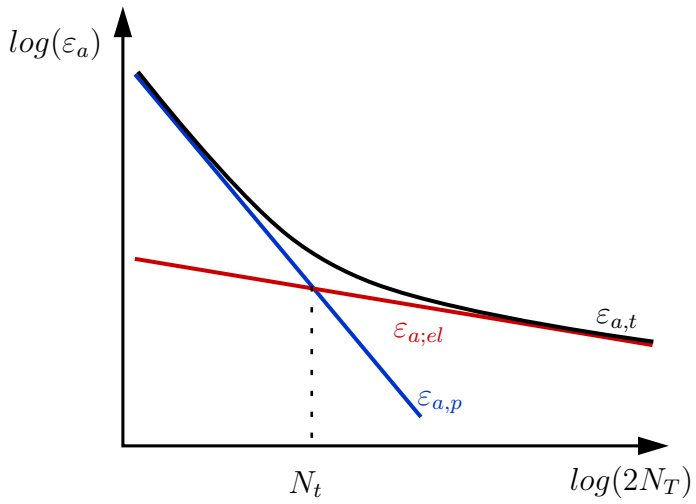

Figure 2.10: Strain life curve without consideration of VHCF regime [Mug13]

With the aid of the material parameters $\sigma_f^{'}$ b, $\varepsilon_f^{'}$ and c, one can determine an approximation of the fatigue behavior, of a specific material. Since many experiments

are needed to determine those parameters, many estimates of those parameters exist. For example, Bäumel, Seeger, and Boller provided the Universal material law (UML) [BSB90], which in practice proved as a valuable method to predict the material parameters as the fatigue parameters for the Equation 2.7 [RHB12][Sur98] .

2.3 Micromechanical simulations

To understand and describe the behavior of metals under cyclic loading, many time-consuming and expensive experiments are required. Furthermore, fatigue is highly influenced by the materials microstructure. One method to take this influence into account is to explicitly take the microstructure into account by micromechanical simulations. These methods compute the local stress and strain fields on the microstructure and derive appropriate measures to model the fatigue damage.
For simulation of local stresses and strains, the Finite element method (FEM) or another computation can be used. The microstructure, therefore, is discretized and described by points in space, which are called nodes. To determine the material response governing equations are solved based on the resulting displacement of the nodes [MGKG17].

For details regarding FEM in micromechanical simmulation see [Boe16, Sch20]. As in our approach, a Fast Fourier Transformation (FFT) solver is used, a short overview of this solver is given. Alternatively to FEM approaches, methods based on the FFT became increasingly popular in the last few years, see Schneider for an overview [SMK17]. Based on the reformulation into a Lippmann-Schiwnger equation, the underlying cell-problem is solved using FFT. This method is based on the work of Moulinec and Suquet [MS94, MS98].

In this work, the commercial FFT solver FeelMath is used [ITW21]. In order to be able to investigate the micromechanical behavior of a metal, a model must be provided. Applying the solver on such models allows determining damage on the microstructure as described in section 3. An example of a generated microstructure, solved by FeelMath, is shown in Figure 2.11 with the resulting von Mises stress.

An Representative volume element (RVE) is a characteristic representation of the microstructure and, therefore, a homogeneous volume element with an arbitrary position in the component. The RVE's mechanical behavior represents the whole material. The RVE's dimension should be just large enough to suitably reflect the stochastic fluctuations of material properties on the pertinent scale [Zem03]. Thus, much compu-

tational time can be saved compared to simulating the whole component. Concerning the scale of one RVE, the length l_{RVE} should be chosen as:

$$l_{elementofmicrostructure} << l_{RVE} << l_{component} \tag{2.8}$$

where the boundaries are caused by physical phenomena on the lower scale and numerical reasons on the upper scale [Boe16]. Furthermore, for the RVE we are using periodic boundary conditions, thus reproducing statistical features of the real microstructure and predict accurately the behavior, while the size of the required RVE is reduced. For further description and requirements regarding RVE, please refer to Zeman [Zem03].

Since the computational cost can be problematic with the appropriate RVE size, long-range influencing factors, such as the damage localization occurring during crack initiation, are carried out via statistical averaging. This averaging is done with statistical volume elements (SVE), which consider short-range influence factors (by statistical microstructure variations).

For the spectral solver, the underyling micorstructure is discretized by voxels. A representation of the microstructure is created by arranging those voxels in a regular grid. The peculiarity of voxels is that each represents the value in a regular grid. Furthermore, the position of each voxel is not directly defined but instead is based upon the position of other voxels creating the regular three-dimensional grid.

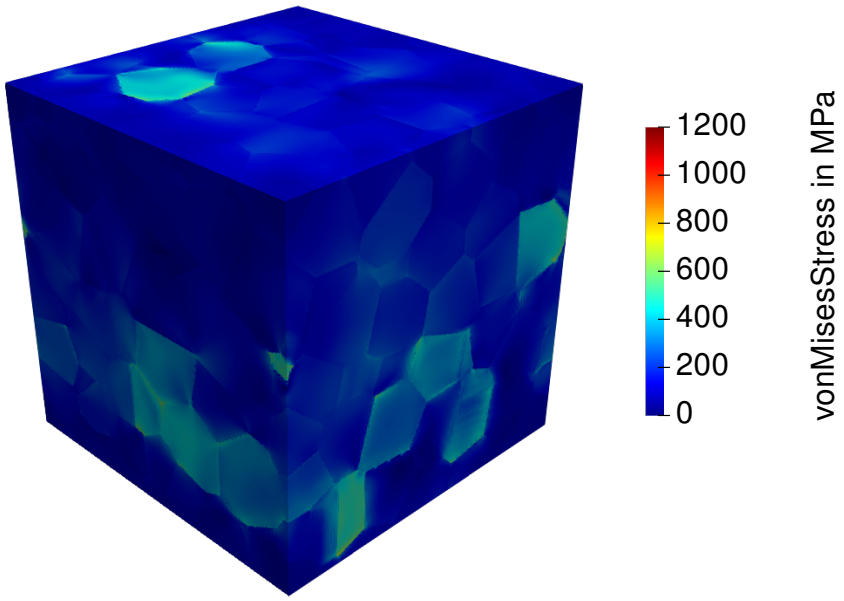

Figure 2.11: Example of microstructure solved with FeelMath

3 Methods

3.1 Microstructure generation

In this work, synthetic representations of the underlying polycrystalline microstructure are used, see Kanit, Matti Schneider [KFG+03, Sch21] for a discussion on why these representations can be beneficial over using experimetnally obtained images. There are multiple ways to create those models. In this section, an understanding of the algorithm, used to create models of the microstructure, is given. In this work we use the algorithm proposed by Kuhn et al. [KSSRB20], which extends the method of Bourne et al. [BKRS20] to create volume elements with prescribed grain sizes. The algorithm can generate an accurate representation of the targeted microstructure, which means that the volume fraction of each grain in the microstructure can be precisely determined. Each grain D_i in the microstructure Y is determined as

$$D_i = \{x \in Y \mid d(x, x_i)^2 - w_i \leq d(x, x_j)^2 - w_j \quad for\ j \in \{1, 2, \cdots, K\}\} \tag{3.1}$$

where w_i is the corresponding weight of each cell. Furthermore, for the weight is applied that the sum of the weights is zero. This weight controls the size of the corresponding Laguerre cell and, following Bourne and Kuhn [BKRS20, KSSRB20], allows the generation of Laguerre tessellation for which the size of each cell can be prescribed.

For positive lengths L_i, a rectangular domain in $\mathbb{R}^d$ as $Y = [0, L1) \times [0, L2) \times \cdots \times [0, L1)$ with periodic boundary condition is defined as our volume of interest (SVE). Each Laguerre cell D_i is part of the unit cell of interest Y. Also a sequence of distinct points $(x_1, x_2, \cdots, x_K) \in Y^K$ lying inside Y as the seed of each cell K with a specified volume fraction is given. For the sequence of the volume fraction $(\phi_1, \phi_2, \cdots, \phi_K) \in \mathbb{R}^K_{>0}$ applies that each value is non-negative, and the sum of the sequence results in $\sum_{i=1}^{K} \phi_i = 1$. The volume fraction for each of the cell is prescribed as

$$\frac{|D_i|}{|Y|} = \phi_i, \tag{3.2}$$

with $|D_i|$ as the volume of each cell $D_1, D_2, \cdots, D_K$. By defining the fundamental parameters, such as the lengths L_i for Y, the number of cells D_i and the volume fraction ϕ_i, the studied microstructure is generated. For a more detailed description

and the theory of convex optimization problems please refer to Kuhn [KSSRB20].

3.2 Crystal plasticity model

The created SVEs are a geometric representation of the microstructure. Now, a suitable model must be assigned to the SVE to determine the microstructure's local deformations. The approach used for this work is the crystal plasticity model (CP). CP models are classified in phenomenological and physics-based models and assume that plastic deformation results from dislocation slip along the slip planes [Sch20]. The phenomenological CP at small strains is used in this work. The advantage of this method is that the results have a sufficient accuracy compared to experimental observations [NDSRM21], while only a few material parameters are needed.
Considering all slip systems N_S, the flow rule as the superposition of crystallographic slips, following Bishop [Bis53], is formulated as:

$$\dot{\varepsilon}_p = \sum_{\alpha=1}^{N_S} \dot{\gamma}^\alpha M^\alpha \tag{3.3}$$

where M^α is the symmetrized Schmid tensor of the slip systems α and enables the projection of the stresses in the system by:

$$M^\alpha = \frac{1}{2}(m^\alpha \otimes n^\alpha + n^\alpha \otimes m^\alpha). \tag{3.4}$$

More precisely the vector n^α encodes the slip plane's normal and thus is orthogonal to the slip direction m^α. M^α is used to calculated the resolved shear stress

$$\tau^\alpha = \sigma \cdot M^\alpha \tag{3.5}$$

of a slip system α, which is activated if τ^α reaches a critical value τ_C^α.

To complete equation 3.3, the system-dependent shear rate can be expressed as a function of the internal states variable,

$$\dot{\gamma}^\alpha = \dot{\gamma}_0 sgn(\tau^\alpha - \chi_b^\alpha) \left| \frac{\tau^\alpha - \chi_b^\alpha}{\tau_c^\alpha} \right|^c \tag{3.6}$$

where χ_b^α is the slip system-dependent back stress, which captures the Bauschinger effect and the ratcheting behavior. This phenomenological visco-plastic flow rule is suggested by Hutchinson. [Hut76]

For a detailed overview of the different material models and modeling approaches based on the CP-Method and further details on the methodology, please refer to Roters et al. [REBR10] instead.

The back stress in Equation 3.6 underlies the phenomena of changed interactions' frequency of dislocation during flow. Those changes of the dislocations manifests itself in the physical hardening of the material as described in subsection 2.2. Since the hardening and dehardening processes are in equilibrium after a certain number of loads, the stabilized constant critical value of the shear stress in Equation 3.6 can be used instead [BfE12].

In the case of recurrent loading, the Bauschinger phenomenon must also be considered. It can be described mathematically, for example, by evolution equations of the back stresses χ_b^α on each sliding system α. These back stresses are then introduced as further state variable into the flow rule (Equation 3.6) and change the resolved shear stress τ^α. The model used in this work, is the formulation of Ohno and Wang [OW93], which is an extension to the formulation of Armstrong and Frederick [FA07]:

$$\dot{\chi}_b^\alpha = A\dot{\gamma}^\alpha - B\left(\frac{|\chi_b^\alpha|}{\frac{A}{B}}\right)^M \chi_b^\alpha|\dot{\gamma}^\alpha|, \tag{3.7}$$

A, B and M here are parameters that control the influence of the associated term. The first term describes the immediate increase of the back stresses in the direction in which shear occurs. However, with further shear, the value of $\dot{\chi}_b^\alpha$ is reduced by the second term, depending on the already present back stresses χ_b^α . This is based on the hypothesis that more distant sections of history have a decreasing influence on the current development of the back stress [RHB19].
The back stress represents the kinemtaic hardening, due to dislocation annihilation and simultaneously dislocation accumulation of an metal. In the following a brief overview the modeling of the kinematic hardening and thus the back stress is described.

The kinematic hardening of metals can be represented in a multiaxial stress state in the form of a yield surface (Figure 3.1). A yield surface describes the stress states in the main normal stress space and the boundary at which plastification of the material occurs, the so-called yield point. If the stress state lies within the yield surface, purely elastic deformation occurs by not fulfilling the yield condition. In isotropic hardening, the yield surface grows symmetrically around the origin when the yield point is

reached. A material that macroscopically isotropic hardens would, therefore, under a load of opposite direction, begin to flow at the same absolute direction as it was at the moment of the previous unloading. The physical cause of this behavior is strain hardening, i.e., the increase in dislocation density impedes further dislocation movement.

With kinematic hardening, the yield-area does not change in dimension or form, instead shifts in the stress area, which is described by the back stress χ and proposed by [Cai92]. The consequence is that the absolute value of yield stress on reversal of one load does not correspond to the absolute value of yield stress. This phenomenon, captured by the back stress tensor, is called the Bauschinger effect and can be seen schematic in Figure 3.1.

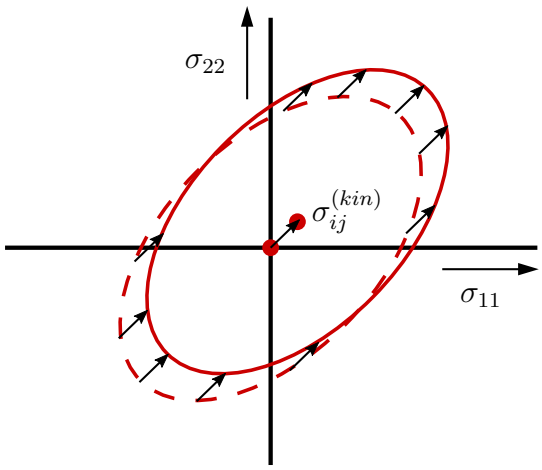

Figure 3.1: Kinematic hardening, evolution of yield surface [RHB19]

3.3 Damage modelling

3.3.1 Fatigue indicator parameter (FIP)

The microstructure model, with consideration of the CP-method, enables the determination of local stresses and strains for each grain. However, the resulting local stresses do not provide directly any information about the fatigue and damage of the metal. Thus, a value for the definition of local damage is required. The damage representing value should allow the estimation of the metal's lifetime with just a small number of simulated load cycles.

In this work, for the measurement of the fatigue damage, fatigue indicator parameters (FIP) are used. FIPs are mesoscopic parameters based on physical considerations [MD10]. The information about the evolution of stress and strain fields during a loading cycle can represent driving forces of fatigue crack nucleation. FIPs consider

the at plastic deformation irreversible slip of glide systems as the foundation for fatigue damage. The most straightforward damage criterion of micromechanical simulations under the assumption of linear accumulated damage is

$$\mathrm{FIP}_{\mathrm{cyc,max}} N_{\mathrm{i}} = \mathrm{FIP}_{\mathrm{crit}} \tag{3.8}$$

with N_{i} as the number of loads till crackinitiation and the critical fatigue parameter $\mathrm{FIP}_{\mathrm{crit}}$. $\mathrm{FIP}_{\mathrm{cyc,max}}$ denotes the biggest FIP for the considered microstructure. The biggest FIP is located at the point $\underline{x}$ at which the most unfavorable loading condition exists. In literature, many FIPs are proposed, and three of them are presented in the following.

Mononukul and Dunne [MD04] introduced the FIP of accumulated plastic slip, based on the statement that small plastic deformations strongly influence fatigue damage in the microstructure. Thus, in every single point in the material $\underline{x}$ a dimensionless scalar is determined as the progression of the plastic slip rate $\dot{\varepsilon}_p(\underline{x})$ for each cycle:

$$\mathrm{FIP}_{cyc,p}(\underline{x}) = \int_{\text{start of cycle}}^{\text{end of cycle}} |\dot{\varepsilon}_p(\underline{x})| \, \mathrm{d}t \tag{3.9}$$

Although this FIP proved useful in many applications [MFK+19, SMML12], one limitation is the disregard of influence of medium stress on crack initiation, which can be observed in experiments [Fin59]. Based on the work of Brown and Miller [BM73], Fatemi and Socie [FS88, Soc93] further developed a FIP, which takes into account the amplitude of plastic slip for each glide system $\Delta\gamma_p^\alpha$ and the normal sstresses in each slip planes σ_n^α.

$$\mathrm{FIP}_{cyc,FS}(\underline{x}) = \max_{\alpha=1\ldots48} \left[\frac{\Delta\gamma_p^\alpha(\underline{x})}{2} \left(1 + k \frac{\sigma_n^\alpha(\underline{x})}{\tau_{c,0}} \right) \right] \tag{3.10}$$

where α describes the different slip systems, i.e., 48 in this work. $\tau_{c,0}$ is the initial critical shear stress, and with the coefficient k, they control the impact of the normal stress on the crack development. The coefficient k depends on the load frequency and controls the influence of the normal stress on the cyclic damage. k becomes smaller with longer lifetimes and converges against one in the HCF [AN02].

Beside the FIPs in Equation 3.9 and Equation 3.10, Korsunsky [KDDW07] presented a FIP driven by the idea of energy dissipation. Korsunsky assumed that by dislocation movement, dissipated energy is directly linked to the fatigue damage due

to the required energy to initiate a crack. In addition to the FIPs mentioned above, there are many other FIPs, but those will not be discussed further.

With the aid of the CP-method, each of the mentioned FIPs can be determined. However, the FIP used in this work is the FIP of accumulated slip (Equation 3.9). For the determination of the lifetime, the resulting FIP needs to be evaluated. Therefore, a critical FIP, for each material and the corresponding FIP, is needed. In the case of the used materials in this work, only the critical FIP of accumulated slip could be determined as described in subsubsection 3.3.3.

3.3.2 Non-Local averaging

The mentioned FIPs in subsubsection 3.3.1 are strongly dependent on the discretization of the SVE, since they are calculated by the CP method in every cell of the SVE. With higher resolution, the initialization point of cracks, which appears in dimensions of sub-micrometers or low μm-range, can be described more precisely. Nevertheless, an averaging over a representative area of the crack incubation zone should be performed, lapsing mesh dependencies regarding fatigue damage [SGM20].
Different methods are used in post-processing to generate those averaged FIPs. One possible method is the band averaging by considering the slip planes of each grain as it is used by Castelluccio [Cas12]. Another more efficient method, which is used in this work, is the sphere averaging method. Boeff [Boe16] showed that with the use of sphere averaging, the mesh dependency is reduced. Local peaks are smeared while deformation trends are captured. For example, he showed that the maximum absolute error in resulting plastic slip between two different finely meshes is reduced from 55% to 5% by using sphere averaging [Boe16].

The resulting $\mathrm{FIP}_\mathrm{i}^*$ for each element $\mathrm{FIP}_\mathrm{i}^*$ by sphere based averaging can be defined by

$$\mathrm{FIP}_\mathrm{i}^* = \frac{1}{V_{pz}} \int_{V_{pz}} \mathrm{FIP}_\mathrm{i} \, \mathrm{d}V \tag{3.11}$$

where, V_{pz} is the process zone Volume for fatigue crack initiation, typically with a diameter in the size of half an equivalent grain size, and FIP_i is the selected FIP. The resulting FIPs are then reassigned to their original integration point. In order to preserve the gradient across grains boundaries, this averaging is spatially done for individual grains [PS18].

3.3.3 Lifetime evaluation

The mentioned FIPs in subsubsection 3.3.1 are dimensionless scalars and do not initially make any statement about the lifetime. Therefore for each FIP a corresponding material specific critical value (FIP_{crit}) is determined. A LCF-experiment at a defined total strain amplitude ($\varepsilon^{\dagger}_{a,t}$) with the fatigue crack initiation lifetime ($N^{\dagger}_{i}$) and a corresponding micromechanical simulation are used to determine FIP_{crit}. A corresponding simulation means to perform at an equal loading as the experiment. The number of cycles in the simulations is chosen so that the resulting FIP is saturated. With consideration of those values the FIP_{crit} can be calculated, as described by Manonukul and Dunne [MD04], with

$$\mathrm{FIP}_{crit} = N^{\dagger}_{i} \cdot \Delta\mathrm{FIP}^{*}_{cyc}(\varepsilon^{\dagger}_{a,t}) \tag{3.12}$$

where $N^{\dagger}_{i}$ is the experimentally observed fatigue lifetime. Taking into account the FIP_{crit} by the assumption of independence concerning the load level and strain ratio, the lifetime of a material can be determined by

$$N_{crit} = \frac{\mathrm{FIP}_{crit}}{\Delta\mathrm{FIP}^{*}_{cyc}} \tag{3.13}$$

where N_{crit} is the critical number of cycles for the microstructure under a defined load until crack initiation and, for that case, the corresponding saturated $\Delta\mathrm{FIP}^{*}_{cyc}$. In this work, the critical values are used for fatigue crack initiation predictions in every range of cycles, based on the hypothesis that the critical FIP keeps constants across regimes, as demonstrated by Manonukul and Dunne [MD04].

Other possible ways are created to determine FIP_{crit}. Sayer described a method to determine the FIP_{crit} by using the parameters introduced by Basquin, Coffin and Manson for empirical fatigue prediction (subsubsection 2.2.2)[SNSRM21]. Thus the FIP_{crit} is calculated with

$$FIP_{crit} = \frac{4\varepsilon'_{f}2^{c}}{\varepsilon_{p,crit}} \tag{3.14}$$

And in turn with it by considering an exponent $m = -1/c$, where c is also a value of empirical fatigue prediction, the lifetime till crack initiation is calculated with

$$N_{crit} = \left(\frac{\mathrm{FIP}_{crit}}{\Delta\mathrm{FIP}^{*}_{cyc}}\right)^{m_{fip}} \tag{3.15}$$

The advantage of this method is, as long as the parameters of the Equation 2.7 can be determined, for example, per UML, the lifetime can be determined. Thus in this work, the lifetime is calculated using the UML and the approach of Sayer [SNSRM21]. Outgoing from this assumption, the comparisons between different phases are done, which describes where a microstructure is expected to fail first.

4 Conclusion

The presented work analyzed the influence of a ferritic phase on the lifetime of a ferritic-martensitic microstructure. The influence of the δ-ferrite volume fraction, the spatial distribution, and the ferrite grain size were investigated.
In the first step, two-phase microstructures were generated. A basic discretization study has shown that a resolution of 64^3 cells correctly reproduces the volume distribution while keeping the computational cost manageable. Furthermore, this study confirmed that the resulting FIPs values are discretization dependent. However, the discretization dependence is diminished due to the sphere averaging applied in post-processing.

When analyzing the influence of the δ-ferrite volume fraction on the fatigue lifetime in a strain-controlled condition, it was found that a small volume fraction of the ferritic phase decreases the lifetime. This could be attributed to the strain-controlled loading and the resulting stress and strain distribution in the mixed-microstructures. For given applied strain, higher stresses are generated in the ferritic phase, which can therefore cause more plastic strain and shorten the lifetime.
In contrast, the volume dependence is reduced and barely noticeable under stress-controlled loading. With a high volume fraction, the microstructure must be strained more to apply the same stress amplitudes. Therefore, the same plastic strains occur in the ferritic phase, resulting in similar lifetimes. Furthermore, it was also found that crack initiation occurs mainly in the ferritic phase. An exception is the microstructures with low ferritic volume fraction (5%) loaded with a low strain amplitude (0.3%), where a crack may also initiate in the martensite.

Investigation of the direction dependence of the cyclic load (orthogonal and parallel to the orientation of the δ-ferrite columns) showed that no significant effect on the lifetime was found. Different load directions on the ferritic columns mainly influenced the scatter of the resulting lifetimes.

The strongest effect on the lifetime was shown for different ferritic grain sizes, assuming that the resistance against plastic deformation increases with decreasing grain size (Hall-Petch). It was shown that the lifetime of the microstructure could be improved by reducing the ferritic grain size. In addition, ferritic grain size was also found to affect martensitic lifetime, which is improved with smaller ferritic grain size. Crack initiation occurs mainly in the ferritic phase with a grain size of $> 8.4\mu m$, but for small ferritic grains, the crack is initiated in the martensitic phase.
Figure 4.1 shows that the size of the ferritic grain has a more significant influence than a change in the volume fraction.

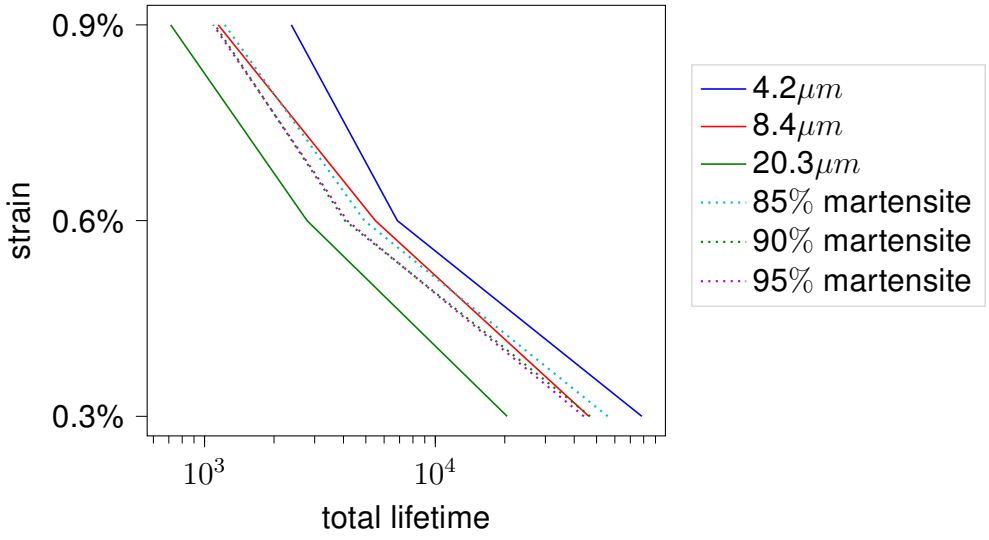

Figure 4.1: Comparison of grain size influence and volume fraction influence. Reference has 90% martensitic volume fraction and a ferritic grain size of $8.4\mu m$

Overall, it was shown for two-phase microstructures that a large difference in the strength of the two phases has a significant damaging effect on the materials fatigue properties. Reducing this strength difference by lowering the grain size of the softer phase can lead to an increase in cyclic lifetime. In addition, it can be concluded that individual large ferrite grains in the area of high stress define the lifetime of a component. It is to be expected that the origin of crack initiation is to be found at large ferritic grains. Thus, when selecting a multiphase metal, it is important to ensure that small grains of the soft phase occur throughout the microstructure.

5 Outlook

In order to consolidate the statements made in this work, it would be beneficial to analyze the evaluations carried out with other FIPs. Therefore, defined experimental data would have to be determined for the individual phases. In addition, correlated simulations must be performed to determine appropriate critical FIPs for each phase and different FIPs. Different FIPs could take into account effects such as the medium stress, which is included in the FIP of the Fatemie and Socie (Section 3.3.1).

The investigations in this thesis refer to crack initiation and therefore do not provide any information about the crack propagation in a multiphase microstructure. A component is usually not considered to have failed with the initiation of a crack, so it would be advantageous to know how the cracks develop and propagate depending

on the multiphase properties. Models would have to be generated to determine the short crack growth depending on the location of initiation and the surrounding grains or phases.

References

[AHL17] Peter M Anderson, John P Hirth, and Jens Lothe. *Theory of dislocations*. Cambridge University Press, 2017.

[AN02] J.A Araújo and D Nowell. The effect of rapidly varying contact stress fields on fretting fatigue. *International Journal of Fatigue*, 24(7):763–775, July 2002.

[Ao74] Sidney H Avner and others. *Introduction to physical metallurgy*, volume 2. McGraw-hill New York, 1974.

[Bas10] OH Basquin. The exponential law of endurance tests. In *Proc Am Soc Test Mater*, volume 10, pages 625–630, 1910.

[BfE12] Wolfgang Bleck and Institut für Eisenhüttenkunde. *Spezielle Werkstoffkunde der Stähle für Studium und Praxis*. 2. 2012.

[Bis53] J. F. W. Bishop. VI. A theoretical examination of the plastic deformation of crystals by glide. *The London, Edinburgh, and Dublin Philosophical Magazine and Journal of Science*, 44(348):51–64, 1953.

[BKRS20] D. P. Bourne, P. J. J. Kok, S. M. Roper, and W. D. T. Spanjer. Laguerre tessellations and polycrystalline microstructures: a fast algorithm for generating grains of given volumes. *Philosophical Magazine*, 100(21):2677–2707, November 2020.

[BM73] M. W. Brown and K. J. Miller. A Theory for Fatigue Failure under Multiaxial Stress-Strain Conditions. *Proceedings of the Institution of Mechanical Engineers*, 187(1):745–755, June 1973.

[BN47] William Lawrence Bragg and J. F. Nye. A dynamical model of a crystal structure. *Proceedings of the Royal Society of London. Series A. Mathematical and Physical Sciences*, 190(1023):474–481, September 1947.

[Boe16] Martin Boeff. *Micromechanical modelling of fatigue crack initiation and growth*. PhD thesis, 2016.

[Bra50] A Bravias. Les Systemes Formes par des Points Distribues Regulierement sur un Plan ou Dans Lespace. *Journal de l'Ecole Polytechnique*, pages 1–128, 1850.

[Bru11] Michiel Brumsen. Case Description: The ICE Train Accident near Eschede. In *Issues in Business Ethics*, volume 28. Springer, Dordrecht, January 2011.

[BSB90] A. Bäumel, T. Seeger, and Chr Boller. Materials data for cyclic loading. *Amsterdam; London; New York, Elsevier*, 1990.

[BSE17] Fabien Briffod, Takayuki Shiraiwa, and Manabu Enoki. Microstructure modeling and crystal plasticity simulations for the evaluation of fatigue crack initiation in α-iron specimen including an elliptic defect. *Materials Science and Engineering: A*, 695:165–177, May 2017.

[Cai92] G. Cailletaud. A micromechanical approach to inelastic behaviour of metals. *International Journal of Plasticity*, 8(1):55–73, January 1992.

[Cas12] Gustavo M. Castelluccio. *A study on the influence of microstructure on small fatigue cracks*. Georgia Institute of Technology. ProQuest Dissertations Publishing, 2012.

[Chr13] Hans-Jürgen Christ. *Wechselverformung von Metallen: zyklisches Spannungs-Dehnungs-Verhalten und Mikrostruktur*, volume 9. Springer-Verlag, 2013.

[Cot54] A. H. Cottrell. Dislocations and Plastic Flow in Crystals. *American Journal of Physics*, 22(4):242–243, April 1954.

[Ell97] Fernand Ellyin. *Fatigue Damage, Crack Growth and Life Prediction*. Springer, Dordrecht, 1 edition, 1997.

[FA07] Charles O Frederick and PJ Armstrong. A mathematical representation of the multiaxial Bauschinger effect. *Materials at High Temperatures*, 24(1):1–26, 2007.

[FCFR20] Harris Farooq, Georges Cailletaud, Samuel Forest, and David Ryckelynck. Crystal plasticity modeling of the cyclic behavior of polycrystalline aggregates under non-symmetric uniaxial loading: Global and local analyses. *International Journal of Plasticity*, 126:102619, March 2020.

[Fin59] W. N. Findley. A Theory for the Effect of Mean Stress on Fatigue of Metals Under Combined Torsion and Axial Load or Bending. *Journal of Engineering for Industry*, 81(4):301–305, November 1959.

[FS88] Ali Fatemi and Darrell F. Socie. A CRITICAL PLANE APPROACH TO MULTIAXIAL FATIGUE DAMAGE INCLUDING OUT-OF-PHASE LOADING. *Fatigue & Fracture of Engineering Materials & Structures*, 11(3):149–165, March 1988.

[Got14] G. Gottstein. *Materialwissenschaft und Werkstofftechnik: Physikalische Grundlagen*. Springer-Lehrbuch. Springer Berlin Heidelberg, 4 edition, 2014.

[HB11] D. Hull and D. J. Bacon. *Introduction to Dislocation*. Elsevier Ltd., Oxford, UK, 5 edition, 2011.

[HHW56] PB Hirsch, RW Horne, and MJ Whelan. LXVIII. Direct observations of the arrangement and motion of dislocations in aluminium. *Philosophical Magazine*, 1(7):677–684, 1956.

[Hut76] Woodside John Hutchinson. Bounds and self-consistent estimates for creep of polycrystalline materials. February 1976.

[ITW21] Fraunhofer ITWM. FeelMath, 2021.

[KDDW07] Alexander M. Korsunsky, Daniele Dini, Fionn P.E. Dunne, and Michael J. Walsh. Comparative assessment of dissipated energy and other fatigue criteria. *Fatigue Damage of Structural Materials VI*, 29(9):1990–1995, September 2007.

[KFG+03] Toufik Kanit, Samuel Forest, Isabelle Galliet, Valérie Mounoury, and Dominique Jeulin. Determination of the size of the representative volume element for random composites: statistical and numerical approach. *International Journal of solids and structures*, 40(13-14):3647–3679, 2003.

[Kru07] U. Krupp. *Fatigue Crack Propagation in Metals and Alloys: Microstructural Aspects and Modelling Concepts*. Wiley, 2007.

[KSSRB20] Jannick Kuhn, Matti Schneider, Petra Sonnweber-Ribic, and Thomas Böhlke. Fast methods for computing centroidal Laguerre tessellations for prescribed volume fractions with applications to microstructure generation of polycrystalline materials. *Computer Methods in Applied Mechanics and Engineering*, 369:113175, September 2020.

[MD04] A Manonukul and F. P. E. Dunne. High– and low–cycle fatigue crack initiation using polycrystal plasticity. 460(2047), July 2004.

[MD10] D. L. McDowell and F. P. E. Dunne. Microstructure-sensitive computational modeling of fatigue crack formation. *International Journal of Fatigue*, 32(9):1521–1542, 2010.

[MFK+19] Kaveh Minaii, Gholam Hossein Farrahi, Morad Karimpour, Hamid Bahai, and Gholam Hossein Majzoobi. Investigation of microstructure effect on

fretting fatigue crack initiation using crystal plasticity. *Fatigue & Fracture of Engineering Materials & Structures*, 42(3):640–650, 2019.

[MGKG17] Karel Matouš, Marc G.D. Geers, Varvara G. Kouznetsova, and Andrew Gillman. A review of predictive nonlinear theories for multiscale modeling of heterogeneous materials. *Journal of Computational Physics*, 330:192–220, February 2017.

[MS94] Herve Moulinec and Pierre Suquet. A fast numerical method for computing the linear and nonlinear mechanical properties of composites. *Comptes rendus de l'Académie des sciences. Série II. Mécanique, physique, chimie, astronomie.*, 1994.

[MS98] H. Moulinec and P. Suquet. A numerical method for computing the overall response of nonlinear composites with complex microstructure. *Computer Methods in Applied Mechanics and Engineering*, 157(1):69–94, April 1998.

[Mug13] Hael Mughrabi. Damage Mechanisms and Fatigue Lives: From the Low to the Very High Cycle Regime. *6th International Conference on Creep, Fatigue and Creep-Fatigue Interaction*, 55:636–644, January 2013.

[NDSRM21] Erik Natkowski, Ali Riza Durmaz, Petra Sonnweber-Ribic, and Sebastian Münstermann. Fatigue lifetime prediction with a validated micromechanical short crack model for the ferritic steel EN 1.4003. *International Journal of Fatigue*, 152:106418, 2021.

[Oro34] E. Orowan. Zur Kristallplastizität. III. *Zeitschrift für Physik*, 89(9):634–659, September 1934.

[OW93] N. Ohno and J.-D. Wang. Kinematic hardening rules with critical state of dynamic recovery, part I: formulation and basic features for ratchetting behavior. *International Journal of Plasticity*, 9(3):375–390, January 1993.

[Pol34] M. Polanyi. Über eine Art Gitterstörung, die einen Kristall plastisch machen könnte. *Zeitschrift für Physik*, 89(9):660–664, September 1934.

[PS18] Veerappan Prithivirajan and Michael D. Sangid. The role of defects and critical pore size analysis in the fatigue response of additively manufactured IN718 via crystal plasticity. *Materials & Design*, 150:139–153, July 2018.

[REBR10] Franz Roters, Philip Eisenlohr, Thomas Bieler, and Dierk Raabe. *Crystal Plasticity Finite Element Methods: In Materials Science and Engineering*. November 2010.

[RHB12] J. Rösler, H. Harders, and M. Bäker. *Mechanisches Verhalten Der Werkstoffe*. Online access with purchase: Springer. Springer Fachmedien Wiesbaden, 2012.

[RHB19] Joachim Rösler, Harald Harders, and Martin Bäker. Plastizität und Versagen. In *Mechanisches Verhalten der Werkstoffe*, pages 65–119. Springer Fachmedien Wiesbaden, Wiesbaden, 2019.

[San13] Michael D. Sangid. The physics of fatigue crack initiation. *Fatigue and Microstructure: A special issue on recent advances*, 57:58–72, December 2013.

[Sch20] Benjamin Josef Schäfer. *Micromechanical modelling of fatigue crack initiation in the martensitic high-strength steel SAE 4150*. doctoralthesis, Ruhr-Universität Bochum, Universitätsbibliothek, 2020. DOI: 10.13154/294-7533.

[Sch21] Matti Schneider. A review of nonlinear FFT-based computational homogenization methods. *Acta Mechanica*, pages 1–50, 2021.

[SGM20] Krzysztof S. Stopka, Tang Gu, and David L. McDowell. Effects of algorithmic simulation parameters on the prediction of extreme value fatigue indicator parameters in duplex Ti-6al-4v. *International Journal of Fatigue*, 141:105865, December 2020.

[SMK17] Matti Schneider, Dennis Merkert, and Matthias Kabel. FFT-based homogenization for microstructures discretized by linear hexahedral elements. *International journal for numerical methods in engineering*, 109(10):1461–1489, 2017.

[SMML12] CA Sweeney, PE McHugh, JP McGarry, and SB Leen. Micromechanical methodology for fatigue in cardiovascular stents. *International Journal of Fatigue*, 44:202–216, 2012.

[SNSRM21] Niklas Sayer, Erik Natkowski, Petra Sonnweber-Ribic, and Sebastian Münstermann. A novel mesoscopic fatigue failure indicator considering plastic reversibility for microstructure-based lifetime simulation. 2021.

[Soc93] D Socie. Critical Plane Approaches for Multiaxial Fatigue Damage Assessment. In DL McDowell and JR Ellis, editors, *Advances in Multiaxial Fatigue*, pages 7–36. ASTM International, West Conshohocken, PA, January 1993. DOI: 10.1520/STP24793S.

[Sur98] S. Suresh. *Fatigue of Materials*. Cambridge Solid State Science. Cambridge University Press, 1998.

[Tay34] Geoffrey Ingram Taylor. The mechanism of plastic deformation of crystals. Part I.—Theoretical. July 1934.

[Wö60] August Wöhler. Versuche zur Ermittlung der auf die Eisenbahnwagenachsen einwirkenden Kräfte und die Widerstandsfähigkeit der Wagen-Achsen. *Zeitschrift für Bauwesen*, 10:583–614, 1860.

[Zem03] Jan Zeman. *Analysis of Composite Materials with Random Microstructure*. 2003.

Institut für Materialprüfung,
Werkstoffkunde und
Festigkeitslehre
Universität Stuttgart
Professor Dr.-Ing. Stefan Weihe

Masterarbeit

durchgeführt bei der	Bosch GmbH	
Ausgabedatum:	1. August 2021	Nr. 760 194
Kandidat:	Roman Hofmann	
Betreuerinnen:	Dr. Petra Sonnweber-Ribic, Yannick Kuhn, M. Sc. | Bosch GmbH Dr. Ewa Soppa, Dr. Christopher Kohler | MPA Universität Stuttgart	

Mikromechanische Ermüdungssimulation: Analyse Phaseneinfluss

In der Bauteilauslegung und Betrachtung von zyklischen Eigenschaften wird häufig ein homogener Werkstoffzustand im Bauteil angenommen. Diese vereinfachte Ansichtsweise ist jedoch bezüglich Rissinitiierung und -wachstum kritisch. Die lokale Gefügestruktur eines Materials kennzeichnet den Schädigungsvorgang unter mechanischer Beanspruchung. Die mikroskopisch auftretenden unterschiedlichen Phasen bestimmen die Rissinitiierung aufgrund ihrer unterschiedlichen mechanischen Materialeigenschaften.

Durch die explizite Abbildung der inhomogenen Mikrostruktur können mithilfe der Kristallplastizität Aussagen über das lokale Schädigungsverhalten getroffen werden. Dabei wird die Kristallstruktur, die Orientierung zur Belastung und Versetzungsbewegungen in Materialgesetzen formuliert, sodass die plastische Verformung einzelner Kristalle durch das Abgleiten von Versetzungsbewegungen nach dem Schubspannungsgesetzt beschrieben werden können.

In der Arbeit soll der Einfluss unterschiedlicher Phasenanteile und deren örtlicher Verteilung auf die Rissinitiierungslebensdauer mithilfe der Kristallplastizitätsmethode untersucht werden.
Dabei sollen folgende Punkte bearbeitet werden:

- Einarbeitung und Literaturrecherche zur Kristallplastizität
- Einarbeitung Mikrostrukturgenerierung
- Literaturrecherche mikromechanische Ermüdungssimulation
- Modellparametrisierung
- Ableiten relevanter Mikrostruktureigenschaften
- Parameterstudie
  - Mikrostrukturgenerierung
  - Volumenanteile
  - Örtliche Verteilung
- Auswertung Schädigungsverhalten

Genehmigt:

Prof. S. Weihe ..... apl. Prof. M. Seidenfuß .....

Projektarbeitsplan

MA Nr.: 760 194 Datum: 31.01.2021

Thema der Arbeit: Mikromechanische Ermüdungssimulation – Analyse Phaseneinfluss

Kandidat: Roman Hofmann **Beginn**: 01.08.2021 **Abgabe**: 31.01.2022

Betreuer: Dr. Ewa Sopppa (IMWF) Dr. Petra Sonnweber-Ribic (Bosch)

Dr. Christoph Kunze (IMWF) Jannick Kuhn (Bosch)

1 Einarbeitung Theoretische Grundlagen

a) Mikrostrukturgenerierung
b) Kristallplastizität
c) Fatigue Indicator Parameters
d) Lebensdauerprognose/Evaluierung

2 Einarbeitung Theoretische Grundlagen

a) Schnittstelle Geometrieerzeugung
b) Schnittstelle Modellgenerierung
c) Schnittstelle Simulationsdurchführung
d) Schnittstelle Evaluierung

3 Untersuchungen

a) Volumenstudie Dehnungskontrolliert
b) Volumenstudie Spannungskontrolliert
c) Einfluss durch Lokalisierung ferritischer Körner
d) Einfluss der ferritischen Korngröße auf Lebensdauer

4 Ausarbeitung

a) Erstellung Diagramme
b) Grundlagen / Methoden und Materialdefinition
c) Auswertung
d) Fazit und Struktur

Teilaufgabe	08.21				09.21				10.21				11.21				12.21				01.22			
1a																								
1b																								
1c																								
1d																								
2a																								
2b																								
2c																								
2d																								
3a																								
3b																								
3c																								
3d																								
4a																								
4b																								
4c																								
4d																								

Erklärung

Ich versichere,

- dass ich meine Arbeit selbständig verfasst habe,
- dass ich keine anderen als die angegebenen Quellen benutzt und alle wörtlich oder sinngemäß aus anderen Werken übernommenen Aussagen als solche gekennzeichnet habe,
- dass die eingereichte Arbeit weder vollständig noch in wesentlichen Teilen, Gegenstand eines anderen Prüfungsverfahrens gewesen ist,
- dass ich die Arbeit weder vollständig noch in Teilen bereits veröffentlicht habe
- dass das elektronische Exemplar mit den anderen Exemplaren übereinstimmt.

.....

Datum Unterschrift